Physics Letters A 377 (2013) 216–221

Contents lists available at SciVerse ScienceDirect

Physics Letters A

www.elsevier.com/locate/pla

Spectrum of localized states in graphene quantum dots and wires

V.V. Zalipaev [a], D.N. Maksimov [b], C.M. Linton [a], F.V. Kusmartsev [c,*]

[a] Department of Mathematical Sciences, Loughborough University, Leicestershire, LE11 3TU, United Kingdom
[b] LV Kirensky Institute of Physics, Krasnoyarsk 660036, Russia
[c] Department of Physics, Loughborough University, Leicestershire, LE11 3TU, United Kingdom

ARTICLE INFO

Article history:
Received 7 September 2012
Received in revised form 5 November 2012
Accepted 6 November 2012
Available online 23 November 2012
Communicated by V.M. Agranovich

Keywords:
High-energy eigenstates
Semiclassical approximation
Generalized Bohr–Sommerfeld quantization condition
Graphene
Tunneling

ABSTRACT

We developed semiclassical method and show that any smooth potential in graphene describing elongated a quantum dot or wire may behave as a barrier or as a trapping well or as a double barrier potential, Fabry–Perot structure, for 1D Schrödinger equation. The energy spectrum of quantum wires has been found and compared with numerical simulations. We found that there are two types of localized states, stable and metastable, having finite life time. These life times are calculated, as is the form of the localized wave functions which are exponentially decaying away from the wire in the perpendicular direction.

1. Introduction

Graphene is the thinnest of existing materials, one atom thick, and consequently very sensitive to its environment. Properties of graphene change drastically depending on the adjacent material, or substrate, and where and how it is deposited [1]. Charged impurities in a SiO_2 substrate can induce an electrostatic potential which may confine electron and hole puddles as observed in [2,3]. The existence of such puddles has a strong influence on electron mobility and conductivity. Here we consider electronic properties of one such puddle having the form of a channel which may be created by an application of a gate voltage to graphene via a metallic strip electrode. It may also be naturally created in epitaxial graphene on SiC due to a terrace step on the SiC layer [4,5]. The positive electrostatic potential due to the atomic terrace on the substrate may form a potential barrier for electrons or a potential well for holes. Such a simple device has many applications, in particular for graphene electronics, and represents a basic element for the fabrication of quantum devices such as a graphene transistor [6].

Since electron and hole quasi-particles may penetrate through any high and wide potential barrier in graphene (Klein tunneling), the existence of bound states is not obvious. This is in contrast with other systems which are described by the conventional Schrödinger equation; for example, a quantum dot confined within a two-dimensional electron gas or a quantum well formed by a GaAs droplet on an AlGaAs substrate. It was first demonstrated in [7] that in graphene a single parabolic barrier is similar to the double barrier potential well in GaAs/AlGaAs [8] and that quasi-bound states exist in this case. The left and right slopes of the parabolic potential barrier act like tunneling barriers. In this Letter we have considered a generic smooth potential and shown clearly for the first time that the lifetime of the quasi-bound states decays exponentially with the thickness of the tunneling barriers. Of particular significance is our discovery of localized bound states and the criterion which determines when the bound states are transformed into the quasi-bound ones.

It is important to note that there is a major difference between rectangular and smooth potential barriers. The presence of stable bound states for a rectangular barrier was first demonstrated in [9]. However, in this case the double barrier structure does not arise and therefore the bound states are always associated with trapping in a potential well. Here we show that similar states can exist in a more generic situation when there is a single 1D smooth potential barrier formed in a graphene monolayer by some external electrostatic potential.

Quasi-particles in graphene [10] and topological insulators [11] are described by the Dirac equation $H\Psi = E\Psi$, with [10, Eq. (19)]:

$$H = v_F(\boldsymbol{\sigma}\cdot\mathbf{p}) + U(x), \tag{1}$$

where the solution $\Psi = (u, v)^{\mathrm{T}}$ is the spinor wave function, $\boldsymbol{\sigma} = (\sigma_1, \sigma_2)^{\mathrm{T}}$, where σ_1 and σ_2 are Pauli matrices, and $\mathbf{p} = -i\hbar\nabla$

* Corresponding author. Tel.: +44 1509 22 33 16.
E-mail address: F.Kusmartsev@lboro.ac.uk (F.V. Kusmartsev).

0375-9601/$ – see front matter
http://dx.doi.org/10.1016/j.physleta.2012.11.028

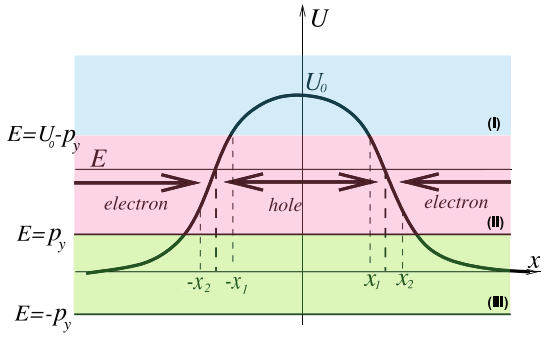

Fig. 1. A typical potential in graphene. The three energy zones, noted in blue (I), red (II) and green (III) are associated with different qualitative behavior. In the blue high energy zone (I) it behaves as a barrier, in the red zone (II) it displays the characteristics of a double barrier structure, while in the green low energy zone (III) it behaves as a potential well localizing both electrons and holes. Quasi-bound (metastable) states are confined by two tunneling strips $(-x_2, -x_1)$ and (x_1, x_2) and are found in the red zone, whereas the bound states are located between $-x_1$ and x_1 and are found in the green zone. (For interpretation of the references to color in this figure legend, the reader is referred to the web version of this Letter.)

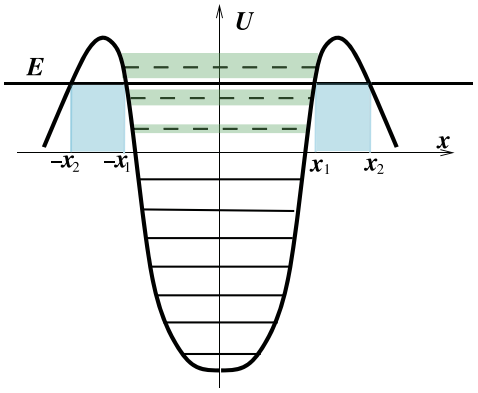

Fig. 2. Schematic shape of a double barrier potential for the 1D Schrödinger equation, equivalent to a double-well Fabry–Perot resonator, which behaves like the smooth potential in graphene presented in Fig. 1 when the energy of quasi-particles belongs to either the red or green zones, i.e. $-p_y < E < U_0 - p_y$. Quasi-bound states shown by dashed lines are confined by two tunneling (blue) strips $(-x_2, -x_1)$ and (x_1, x_2). The width of these energy levels is shown by green strips. (For interpretation of the references to color in this figure legend, the reader is referred to the web version of this Letter.)

is the two-dimensional momentum operator. The two components u and v correspond to the A and B honeycomb sublattices of graphene, respectively, v_F is the Fermi velocity, U is an external potential. Below we consider a class of one-dimensional smooth potentials $U = U(x)$ which have a maximum, $U(0) = U_0$, and vanish at infinity (see Fig. 1). We introduce dimensionless rescaled variables: $x/D \to x$, D being a characteristic length scale for the external potential, $E/U_0 \to E$, $v_F p_y/U_0 \to p_y$, where p_y is the orthogonal component of momentum which we assume to be positive, and $U(x/D)/U_0 \to U(x)$. The WKB solution will be valid when the dimensionless parameter $h = \hbar v_F/U_0 D$ is such that $h \ll 1$. Typical values of U_0 and D are in the ranges 10–100 meV and 100–500 nm. For example, for $U_0 = 100$ meV, $D = 66$ nm, we have $h = 0.1$. Dimensionless variables are used throughout this Letter.

2. Properties of arbitrary smooth potential

It is remarkable that any smooth potential of this kind may behave as a potential well, as a barrier, or as a double well structure; the type of behavior depending on the energy and the direction of the incident wave. Let $p_y \geqslant 0$. There are three energy zones: (I) the "blue" zone, when $U_0 - p_y < E < U_0 + p_y$, (II) the "red" zone, when $p_y < E < U_0 - p_y$ and (III) the lowest energy, "green" zone, when $|E| < p_y$ (see Fig. 1). The energy value $E = p_y$ is the cut-off energy. For $|E| < p_y$ there are no propagating waves outside the potential. For the sake of simplicity we assume that the smooth potential has a symmetric shape.

If the energy of incident quasi-particles belongs to the red zone there are four turning points $\pm a$, $\pm b$ (zone (II) in Fig. 1 where $x_1 = a$ and $x_2 = b$), given by the solutions of the equation

$$p_x = \sqrt{\big(U(x) - E\big)^2 - p_y^2} = 0, \tag{2}$$

since we deal with the Hamiltonian $H = U \pm \sqrt{p_x^2 + p_y^2}$.

Here the smooth potential acts much like the double barrier structure for 1D Schrödinger equation presented in Fig. 2. There may be five different domains of the different particle's behavior: (1) $x < -b$, (2) $-b < x < -a$, (3) $-a < x < a$, (4) $a < x < b$ and (5) $b < x$. Within the classically forbidden domains $(-b < x < -a$ and $a < x < b)$ the solution is a combination of exponentially decaying and growing contributions and these provide coupling between three classically allowed domains associated with oscillatory solutions. Matching solutions found independently for these five domains results in WKB equations for the transfer matrix that, in turn, gives the transmission and reflection coefficients of the electron scattering over this barrier in graphene.

In the green energy zone, $|E| < p_y$ (band (III) in Fig. 1) the effective double barrier structure disappears and only one potential well arises. There is no wave propagation outside this well, however there are oscillatory solutions within. They are associated with stable bound states as in a rectangular barrier [9]. For other shapes of the barriers different approaches have been developed [12–14].

Now, consider the spectral problem for the smooth barrier within the red energy zone: $p_y < E < U_0 - p_y$ where all four turning points are present. Here we observe incident, reflected and transmitted electronic states at $x < -a$ and $x > a$, whereas under the barrier $-a < x < a$ we have a hole state. On the basis of the semiclassical asymptotic analysis developed in [13] it has been pointed out that for $p_y > 0$ total transmission takes place only for a symmetric barrier.

When $h^{-1/2}(b-a) \gg 1$ all four turning points are separate then there is a tunneling barrier on each side of the potential. This phenomenon is similar to a 1D Fabry–Perot resonator which is well described by a 1D Schrödinger equation with the double-well potential shown in Fig. 2 and has both localized and metastable states. The latter have a complex energy spectrum with $\mathrm{Re}(E_n) > 0$, $\mathrm{Im}(E_n) < 0$ (shown by dashed lines in Fig. 2). The states localized inside the potential well have a real spectrum with $E_n < 0$ (solid lines in Fig. 2). If $p_y \to 0$ (normal incidence) the turning points, a and b, coalesce, and all localized states disappear. Note that in the case of normal incidence one observes total transmission (Klein tunneling).

3. WKB asymptotic solution for Dirac system in classically allowed domain

The WKB oscillatory asymptotic solution to the Dirac system in the classically allowed domains is to be sought in the form of asymptotic series (see [15,16]) with real $S(x)$

$$\psi = \begin{pmatrix} u \\ v \end{pmatrix} = e^{\frac{i}{h}S(x)} \sum_{j=0}^{+\infty} (-ih)^j \begin{pmatrix} u_j \\ v_j \end{pmatrix} = e^{\frac{i}{h}S(x)} \sum_{j=0}^{+\infty} (-ih)^j \psi_j(x). \tag{3}$$

Substituting this series into the Dirac system, and equating to zero corresponding coefficients of successive degrees of the small

parameter h, we obtain a recurrent system of equations which determines the unknown $S(x)$ (classical action) and $\psi_j(x)$, namely,

$$(H-EI)\psi_0=0,\qquad (H-EI)\psi_j=-R\psi_{j-1},\quad j>0, \tag{4}$$

$$H=\begin{pmatrix} U(x) & p_x-ip_y\\ p_x+ip_y & U(x)\end{pmatrix},\qquad \widehat{R}=\begin{pmatrix}0 & \partial_x\\ \partial_x & 0\end{pmatrix}, \tag{5}$$

where I is the identity matrix and $S'=p_x$. The Dirac Hamiltonian H has two eigenvalues

$$h_{1,2}=U(x)\pm\sqrt{p_x^2+p_y^2}\equiv U(x)\pm p$$

and

$$e_{1,2}=\frac{1}{\sqrt{2}}\begin{pmatrix}1\\ \pm\frac{p_x+ip_y}{p}\end{pmatrix}$$

with

$$p_x=\pm\sqrt{\big(E-U(x)\big)^2-p_y^2}.$$

From now on we will omit the dependence on x of U, S, and quantities derived from them. It turns out to be convenient to use different $e_{1,2}$ instead with

$$e_{1,2}=\frac{1}{\sqrt{2}}\begin{pmatrix}1\\ \pm e^{i\theta}\end{pmatrix},\qquad e^{i\theta}=\frac{p_x+ip_y}{E-U}.$$

In this way we will be able to solve problems of electron and hole incidence on the barrier simultaneously. Note that, irrespective of whether $E>U$ or $E<U$,

$$He_1=Ee_1,\qquad He_2=(2U-E)e_2. \tag{6}$$

The classical action $S(x)$ is given by

$$S=\int p_x\,dx=\pm\int\sqrt{(E-U)^2-p_y^2}\,dx, \tag{7}$$

the sign indicating the direction of the wave, with + corresponding to a wave traveling to the right.

For electrons and holes one can seek a solution to the Dirac system zero-order problem in the form

$$\psi_0=\sigma^{(0)}(x)e_1 \tag{8}$$

with unknown amplitude $\sigma^{(0)}$. The solvability of the problem $(H-EI)\psi_1=-\widehat{R}\psi_0$ requires that the orthogonality condition $\langle e_1,\widehat{R}(\sigma^{(0)}e_1)\rangle=0$ must hold, written as a scalar product implied with complex conjugation, and from this one obtains the transport equation for $\sigma^{(0)}$:

$$\frac{d\sigma^{(0)}}{dx}\big(e^{i\theta}+e^{-i\theta}\big)+\sigma^{(0)}\frac{de^{i\theta}}{dx}=0. \tag{9}$$

It has a solution

$$\sigma^{(0)}=\frac{c_0}{\sqrt{2\cos\theta}}e^{-i\theta/2}$$

with $c_0=const$, where a branch of the analytic function $\sqrt{z}$ is taken that satisfies the condition $\mathrm{Im}(\sqrt{z})\geqslant 0$, $z\in\mathbb{C}$. Below we assume that $p_x>0$, corresponding to a wave traveling in the positive x-direction. Thus, to the leading order we have

$$\psi=\begin{pmatrix}u\\ v\end{pmatrix}=\frac{e^{\pm\frac{i}{h}S_p(x,x_i)}}{\sqrt{J_p^{\pm}}}c_0e_1^{\pm}\big(1+O(h)\big), \tag{10}$$

$$S_p(x,x_i)=\int_{x_i}^{x}p_x\,dt,\qquad J_p^{\pm}=1+e^{2i\theta^{\pm}},\qquad e_1^{\pm}=\frac{1}{\sqrt{2}}\begin{pmatrix}1\\ e^{i\theta^{\pm}}\end{pmatrix},$$

$$e^{i\theta^{\pm}}=\frac{\pm p_x+ip_y}{E-U}.$$

This asymptotic approximation is not valid near turning points where $S'=0$ (see Fig. 1) where $e^{i\theta}=\pm i$ and $\cos\theta=0$. The WKB asymptotic solution, derived in this section, is valid for the domains Ω_i, $i=1,3,5$.

4. Solution in classically disallowed domain

The WKB asymptotic solution to the Dirac system in the classically disallowed domain is to be sought in the form of asymptotic series (see [15,16])

$$\psi=\begin{pmatrix}u\\ v\end{pmatrix}=e^{-\frac{1}{h}S(x)}\sum_{j=0}^{+\infty}(-ih)^j\begin{pmatrix}u_j\\ v_j\end{pmatrix}=e^{-\frac{1}{h}S(x)}\sum_{j=0}^{+\infty}(-ih)^j\psi_j(x), \tag{11}$$

with $S(x)$ real. As in Section 3, we obtain a recurrent system of equations which determines the unknown $S(x)$ and $\psi_j(x)$, namely,

$$(H-EI)\psi_0=0,\qquad (H-EI)\psi_j=-R\psi_{j-1},\quad j>0, \tag{12}$$

$$H=\begin{pmatrix}U & i(q_x-p_y)\\ i(q_x+p_y) & U\end{pmatrix}, \tag{13}$$

where $S'=q_x$, and the matrix R is as in (5). The Hamiltonian H is not Hermitian. It has two eigenvalues and not orthogonal eigenvectors $Hl_{1,2}=h_{1,2}l_{1,2}$, where

$$h_{1,2}=U(x)\pm\sqrt{p_y^2-q_x^2},\qquad l_{1,2}=\begin{pmatrix}1\\ \pm i\sqrt{\frac{q_x+p_y}{p_y-q_x}}\end{pmatrix}$$

as we have

$$i\frac{q_x+p_y}{E-U}=\pm i\sqrt{\frac{q_x+p_y}{p_y-q_x}},$$

where $q_x=\pm\sqrt{p_y^2-(E-U)^2}$, $|q_x|<p_y$. Thus, the function $S(x)$ in a classically disallowed domain is given by

$$S=\int q_x\,dx=\pm\int\sqrt{p_y^2-(E-U)^2}\,dx. \tag{14}$$

Again, for the sake of simplicity, we shall use different $l_{1,2}$

$$l_{1,2}=\frac{1}{\sqrt{1+\kappa^2}}\begin{pmatrix}1\\ \pm i\kappa\end{pmatrix}=\begin{pmatrix}\cos\phi\\ \pm i\sin\phi\end{pmatrix}, \tag{15}$$

where

$$\kappa=\frac{q_x+p_y}{E-U},\qquad \kappa=\tan\phi,\quad -\frac{\pi}{2}<\phi<\frac{\pi}{2}.$$

For electrons and holes one can seek a solution to the Dirac system zero-order problem in the form

$$\psi_0=\sigma^{(0)}(x)l_1 \tag{16}$$

with unknown amplitude $\sigma^{(0)}$. Solvability of the problem $(H-EI)\psi_1=-\widehat{R}\psi_0$ requires that the orthogonality condition must hold $\langle l_1^*,\widehat{R}(\sigma^{(0)}l_1)\rangle=0$, where

$$l_1^*=\frac{1}{\sqrt{1+\kappa^2}}\begin{pmatrix}\kappa\\ i\end{pmatrix}=\begin{pmatrix}\sin\phi\\ i\cos\phi\end{pmatrix}.$$

The vector l_1 is the eigenvector of H, whereas l_1^* is the eigenvector of H^*. From the orthogonality condition one obtains the transport equation for $\sigma^{(0)}$

$$\frac{d\sigma^{(0)}}{dx}-\sigma^{(0)}\tan 2\phi\frac{d\phi}{dx}=0. \tag{17}$$

It has a solution

$$\sigma^{(0)} = \frac{c_0}{\sqrt{-\cos 2\phi}} = c_0\sqrt{\frac{\kappa^2+1}{\kappa^2-1}}, \quad c_0 = const. \tag{18}$$

Below we assume that $q_x > 0$. Thus, to the leading order in classically disallowed domains we have

$$\psi = \frac{e^{\mp\frac{1}{h}S_q(x,x_i)}}{\sqrt{J_q^{\pm}}} l_1^{\pm}\big(1+O(h)\big), \tag{19}$$

where

$$S_q(x,x_i) = \int_{x_i}^{x} q_x\,dt, \qquad J_q^{\pm} = \pm\big((\kappa^{\pm})^2-1\big),$$

$$l_1^{\pm} = \begin{pmatrix} 1 \\ i\kappa^{\pm} \end{pmatrix},$$

and

$$\kappa^{\pm} = \frac{\pm q_x + p_y}{E-U}.$$

This asymptotic approximation is not valid near turning points $q_x = 0$. The WKB asymptotic solution, derived in this section, is valid for the domains Ω_i, $i = 2, 4$.

5. WKB asymptotic solution for scattering through the smooth barrier

Consider a problem of scattering through the smooth barrier (see Fig. 1). From the point of view of physics of graphene, if $E > 0$ we observe incident, reflected and transmitted electronic states at $x < a$ and $x > b$, whereas under the barrier $a < x < b$ we have a hole state (n–p–n junction, see Fig. 1).

To formulate the scattering problem for transfer matrix T, here we present the WKB solutions in the domains 1 and 5

$$\psi_1 = \frac{e^{\frac{i}{h}S_p(x,x_1)}}{\sqrt{J_p^+}} a_1 e_1^+ + \frac{e^{-\frac{i}{h}S_p(x,x_1)}}{\sqrt{J_p^-}} a_2 e_1^-, \tag{20}$$

$$\psi_5 = \frac{e^{\frac{i}{h}S_p(x,x_4)}}{\sqrt{J_p^+}} d_1 e_1^+ + \frac{e^{-\frac{i}{h}S_p(x,x_4)}}{\sqrt{J_p^-}} d_2 e_1^-. \tag{21}$$

The barrier is represented by the combination of the left and right slopes. The total transfer matrix T, that is $d = Ta$, is given by

$$T = T^R \begin{pmatrix} e^{\frac{i}{h}P} & 0 \\ 0 & e^{-\frac{i}{h}P} \end{pmatrix} T^L, \tag{22}$$

where

$$P = \int_{-a}^{a} \sqrt{\big(U(x)-E\big)^2 - p_y^2}\,dx$$

and T^R and T^L the transfer matrices of the right and left slopes, respectively. Their semiclassical asymptotic description is to be found in [13]. The entries of the matrix T read

$$T_{11} = e^{2\frac{Q}{h}}\big[s^2 e^{i(2\theta+\frac{P}{h})} + e^{-i\frac{P}{h}}\big], \tag{23}$$

$$T_{22} = e^{2\frac{Q}{h}}\big[s^2 e^{-i(2\theta+\frac{P}{h})} + e^{i\frac{P}{h}}\big], \tag{24}$$

$$T_{12} = T_{21} = -2se^{2\frac{Q}{h}}\cos\left(\theta+\frac{P}{h}\right), \tag{25}$$

$$Q = \int_a^b \sqrt{p_y^2 - \big(U(x)-E\big)^2}\,dx,$$

$$\theta = \frac{Q}{\pi h}\left(1-\log\left(\frac{Q}{\pi h}\right)\right) - \frac{\pi}{4} - \arg\Gamma\left(1-i\frac{Q}{\pi h}\right), \tag{26}$$

where $s = \sqrt{1-e^{-2Q/h}}$, $\Gamma(z)$ is the Gamma function. They satisfy the classical properties of transfer matrix $T_{22} = T_{11}^*$, $T_{21} = T_{12}^*$, $\det T = 1$, and if $a_1 = 1$, $a_2 = r_1$, $d_1 = t_1$, $d_2 = 0$, then $t_1 = 1/T_{22}$, $r_1 = -T_{21}/T_{22}$, $|t_1|^2 + |r_1|^2 = 1$. If $a_1 = 0$, $a_2 = t_2$, $d_1 = r_2$, $d_2 = 1$, then $t_2 = t_1 = t$, $r_2(p_y) = T_{12}/T_{22}$, $|t_2|^2 + |r_2|^2 = 1$.

Correspondingly, the unitary scattering matrix that connects

$$\begin{pmatrix} a_2 \\ d_1 \end{pmatrix} = \hat{S}\begin{pmatrix} a_1 \\ d_2 \end{pmatrix}$$

may written as follows

$$\hat{S} = \begin{pmatrix} r_1 & t \\ t & r_2 \end{pmatrix}.$$

The transmission coefficient $t = 1/T_{22}$, looks exactly like the formula (131) in [13]

$$t = e^{i\theta}\left(\cos\left(\frac{P}{h}+\theta\right)\big(2e^{\frac{2Q}{h}}-1\big) + i\sin\left(\frac{P}{h}+\theta\right)\right)^{-1}. \tag{27}$$

The reflection coefficients is given by

$$r_1(p_y) = \frac{2\,\mathrm{sgn}(p_y)\cos(\frac{P}{h}+\theta)e^{\frac{2Q}{h}+i\theta}\sqrt{1-e^{-2Q/h}}}{\cos(\frac{P}{h}+\theta)(2e^{\frac{2Q}{h}}-1) + i\sin(\frac{P}{h}+\theta)}. \tag{28}$$

It is clear that if

$$P(E) = h\left(\pi\left(n+\frac{1}{2}\right)-\theta\right), \quad n = 0, 1, 2, \ldots, \tag{29}$$

than we have that the total transmission, $|t| = 1$.

6. Solution for complex resonant (quasi-bound) states localized within the smooth barrier

Consider a problem of resonant states localized within the smooth barrier (see Fig. 2). In the first case when the energy of the electron–hole is greater than the cut-off energy ($E \geqslant |p_y|$), we have 5 domains Ω_i, $i = 1, 2, \ldots, 5$, and 5 WKB forms of solution to the leading order. Due to the localization of the WKB solution as $x \to \pm\infty$ one should determine the correct radiation conditions in the domains 1 and 5, namely

$$\psi_1 = \frac{e^{-\frac{i}{h}S_p(x,x_1)}}{\sqrt{J_p^-}} a_2 e_1^-, \qquad \psi_5 = \frac{e^{\frac{i}{h}S_p(x,x_4)}}{\sqrt{J_p^+}} d_1 e_1^+. \tag{30}$$

For complex values of E these exponential functions decay as $x \to \pm\infty$. Thus, the other two coefficients should satisfy $a_1 = 0$, $d_2 = 0$ as the corresponding exponential functions blow up. Since $d_2 = T_{21}a_1 + T_{22}a_2$, then

$$T_{22}(E) = 0, \tag{31}$$

and as a result we obtain Bohr–Sommerfeld quantization condition for complex energy eigen-levels (quasi-discrete)

$$P(E) = h\left(\pi\left(n+\frac{1}{2}\right) - \theta - \frac{i}{2}\log\big(1-e^{\frac{-2Q}{h}}\big)\right),$$
$$n = 0, 1, 2, \ldots, N_1 \tag{32}$$

for $|p_y| < E < U_0$. Solutions to this equation are complex resonances $E_n = \mathrm{Re}(E_n) - i\Gamma_n$, where Γ_n^{-1} is the lifetime of the localized resonance. What is important is that the real part of these complex positive resonances is decreasing with n, thus showing off the anti-particle hole-like character of the localized modes. For these resonances we have $\Gamma_n > 0$. From (32), we obtain the important estimate

$$\Gamma_n = \frac{hw}{2\Delta t},$$
$$w = -\log\left(1 - e^{-2Q/h}\right), \quad \Delta t = -P'(E_n), \tag{33}$$

where $P'(E)$ is the derivative of the function $P(E)$.

For the second set of real resonances, when the energy of the electron–hole is smaller than the cut-off energy ($E < |p_y|$), we have 2 turning points $-a$ and a. Between them we have got oscillatory WKB solutions

$$\psi_1 = \frac{e^{\frac{i}{h}S_p(x,x_2)}}{\sqrt{J_p^+}}\bar{d}_1 e_1^+ + \frac{e^{-\frac{i}{h}S_p(x,x_2)}}{\sqrt{J_p^-}}\bar{d}_2 e_1^-, \tag{34}$$

or

$$\psi_1 = \frac{e^{\frac{i}{h}S_p(x,x_3)}}{\sqrt{J_p^+}}\bar{a}_1 e_1^+ + \frac{e^{-\frac{i}{h}S_p(x,x_3)}}{\sqrt{J_p^-}}\bar{a}_2 e_1^-, \tag{35}$$

and outside decaying

$$\psi_1 = \frac{e^{\frac{1}{h}S_q(x,x_2)}}{\sqrt{J_q^-}}\bar{c}_2 l_1^-, \quad x < x_2,$$
$$\psi_3 = \frac{e^{-\frac{1}{h}S_q(x,x_3)}}{\sqrt{J_q^+}}\bar{c}_1 l_1^+, \quad x > x_3. \tag{36}$$

By gluing these WKB solutions through the two boundary layers near $-a$ and a, we eliminate $\bar{a}_{1,2}$ and $\bar{d}_{1,2}$ and obtain the homogeneous system of equations

$$i\bar{c}_1 + \bar{c}_2 e^{i/hP} = 0, \qquad i\bar{c}_1 - \bar{c}_2 e^{-i/hP} = 0.$$

Thus, we derive the Bohr–Sommerfeld quantization condition for real energy eigen-levels (bound states) inside the cut-off energy strip for $0 < E < |p_y|$.

$$P(E) = h\pi\left(n + \frac{1}{2}\right), \quad n = N_1 + 1, \ldots, N_2. \tag{37}$$

7. Comparison between quasi-classical and numerical solutions

For other non-rectangular shapes of the barriers there are different approaches which have been developed in Refs. [12–14]. Here, we have solved the Dirac equation, with the Hamiltonian (1) for a typical specific potential $U(x) = 1/\cosh x$, which may describe a quantum wire or very elongated quantum dot. The Energy Domain Finite Difference (FD) Method and the truncation technique with the use of absorbing boundary conditions have been applied to build a finite size FD lattice model. For each selected p_y we computed the response of the FD lattice model. The amplitude vs energy response was then processed with the harmonic inversion method (see [17] for details) to obtain the positions and widths of the resonances.

The results for the energy spectrum and eigenfunctions obtained from analytical semiclassical expressions, see (31), were compared with the ones computed numerically. Fig. 3 shows the dispersion of energy levels $E_n(p_y)$ as a function of p_y for complex resonant and real bound states with quantum numbers

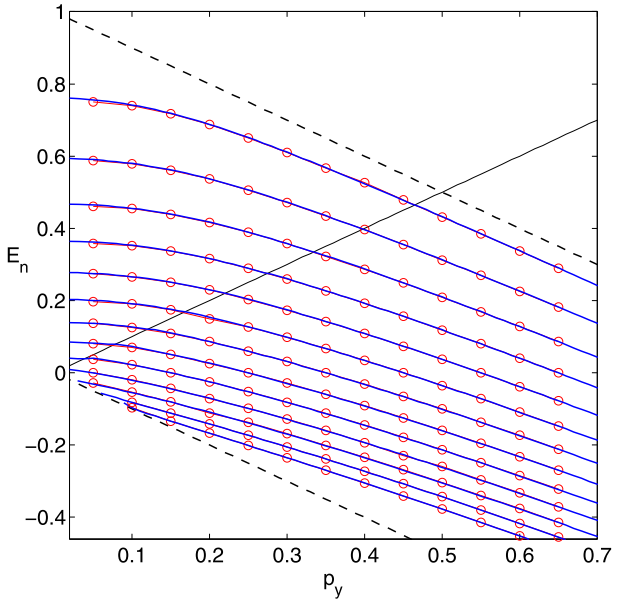

Fig. 3. The real part E_n of first 13 eigenvalues. Semiclassical solutions are shown by blue lines and numerical results by red circles. The upper and lower bounds for dispersion branches are shown by thin dotted lines. The faint black line $p_y = E$ is the upper bound for the bound states where $\Gamma_n = 0$. (For interpretation of the references to color in this figure legend, the reader is referred to the web version of this Letter.)

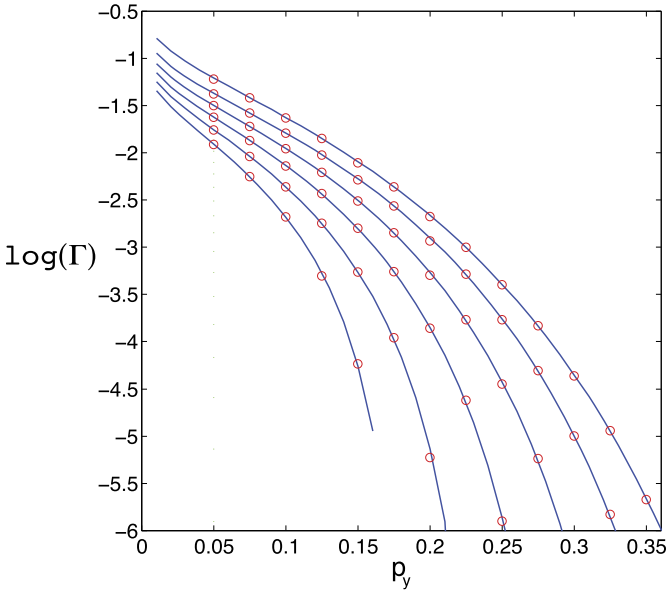

Fig. 4. The imaginary part of $\mathrm{Log}\,\Gamma_n$ of the first 6 quasi-bound eigenvalues. Semiclassical solutions are shown by blue lines and numerical results by red circles. (For interpretation of the references to color in this figure legend, the reader is referred to the web version of this Letter.)

$n = 0, 1, \ldots, 12$ and $h = 0.1$. For complex resonant states only the real part is shown. We found that for quantum numbers $n = 0, 1, \ldots, 8$ the imaginary parts, $\Gamma_n(p_y)$, of complex resonant bound states also depend on the value of p_y as demonstrated in Fig. 4. The complex quasi-bound states exist within the red energy zone (II), i.e. $p_y < E < U_0 - p_y$, whereas the real bound states exist in the low energy, green zone (III) or in the strip of the (E, p_y) plane determined by $E < U_0 - p_y$, $-p_y < E < p_y$ (see Figs. 1, 3).

In Fig. 5 we present a color plot for the transmission coefficient, $|t|^2$, through the same barrier with respect to p_y and

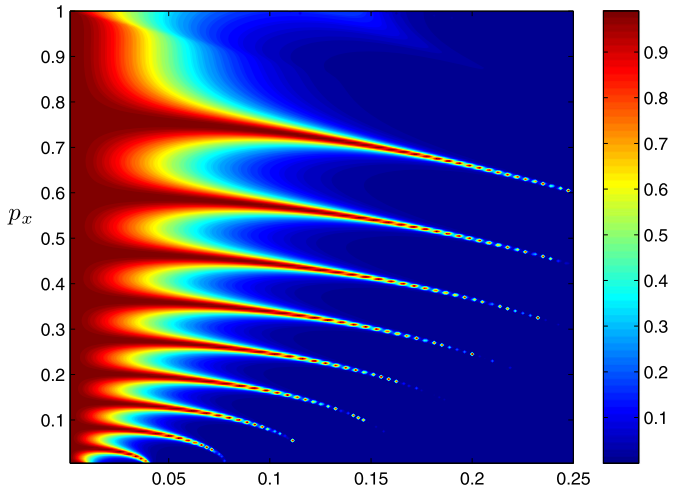

Fig. 5. Transmission probability $|t|^2$ colorbar diagram with respect to p_y and $p_x = \sqrt{E^2 - p_y^2}$ for $U = 1/\cosh x$.

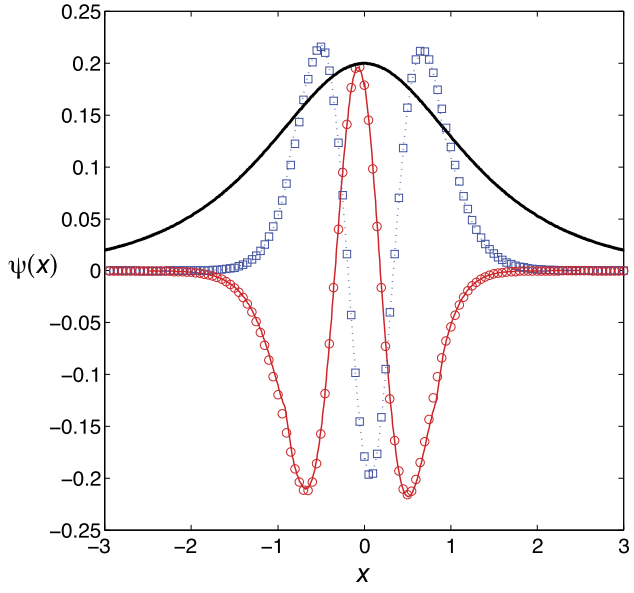

Fig. 6. The form of the wave function for the localized solution for $p_y = 0.5$ and quantum number $n = 2$. The real part of the first component of the Dirac spinor, u, is shown by the red solid line; the imaginary part of the second component, v, by blue dotted line. Corresponding numerical results are shown by circles and squares. The potential $\frac{1}{5}U(x)$ is plotted as a black solid line to pinpoint the localization area. (For interpretation of the references to color in this figure legend, the reader is referred to the web version of this Letter.)

$p_x = \sqrt{E^2 - p_y^2}$. The most intense red color corresponds to the resonance transmission when $|t| = 1$. The number of these resonances is 9 corresponding to the number of complex quasi-bound states shown in the red zone (II) determined by $p_y < E < U_0 - p_y$; see Figs. 1 and 3. All bound states have infinite lifetime. All states are confined within the barrier in the x-direction while the motion in the y-direction is described by plane waves; the energy–momentum relation is controlled by (31). In all figures we see a very good agreement between the quasi-classical theory and the numerical experiments. When $p_y \to 0$ the resonance widths go to infinity and the lifetime vanishes due to the Klein paradox.

As an example we present the shape of the wave function in Fig. 6, where we plotted the real part of u component and the imaginary part of v component obtained using WKB approximations, and also make a comparison with numerical data. For both methods the results have been calculated for the third energy–momentum dispersion branch, i.e. $n = 2$ at the value $p_y = 0.5$ (see the spectrum given in Fig. 3). Again one observe a good coincidence between semiclassical and numerical results.

In summary, we have applied a semiclassical analysis of Dirac electron or hole tunneling through a smooth potential in grapheme. We show that this potential may act as a barrier, as a trapping well or as the double barrier, Fabry–Perot structure. For the first time we describe the localized and quasi-bound states and have determined their spectrum. We have also presented a new, more detailed description of the quasi-bound states noted in [7] and, in particular, have derived precise expressions for their life times. Quasi-bound states undergo a transition into completely bound states as their life time tends to infinity. The semiclassical equations have been compared with numerical simulations taken for a specific but typical potential describing quantum dots or quantum wires in graphene. The comparison shows excellent agreement. The fact that any potential in graphene can induce both stable and metastable states may have a significant consequences on the operation of various graphene-electronic devices.

Acknowledgements

V. Zalipaev acknowledges helpful discussion with Alex Vagov and D. Maksimov would like to thank A.F. Sadreev for useful discussions.

References

[1] A. O'Hare, F.V. Kusmartsev, K.I. Kugel, Nano Lett. 12 (2012) 1045.
[2] J. Martin, et al., Nature Phys. 4 (2008) 144.
[3] J. Martin, et al., Nature Phys. 5 (2009) 669.
[4] P. Sutter, Nature Mater. 8 (2009) 171.
[5] J. Robinson, et al., ACS Nano 4 (2010) 153, PMID: 20000439.
[6] Y.-M. Lin, et al., IEEE Electron Device Lett. 32 (2011) 1343.
[7] P.G. Silvestrov, K.B. Efetov, Phys. Rev. Lett. 98 (2007) 016802.
[8] K. Leo, et al., Phys. Rev. Lett. 66 (1991) 201.
[9] J.M. Pereira, V. Mlinar, F.M. Peeters, P. Vasilopoulos, Phys. Rev. B 74 (2006) 045424.
[10] A.H. Castro Neto, F. Guinea, N.M.R. Peres, K.S. Novoselov, A.K. Geim, Rev. Mod. Phys. 81 (2009) 109.
[11] F.V. Kusmartsev, A.M. Tsvelick, JETP Lett. 42 (1986) 257.
[12] E.B. Sonin, Phys. Rev. B 79 (2009) 195438.
[13] T. Tudorovskiy, K.J.A. Reijnders, M.I. Katsnelson, Physica Scripta 2012 (2012) 014010.
[14] P. Markoš, C.M. Soukoulis, Wave Propagation. From Electrons to Photonic Crystals and Left-Handed Materials, Princeton University Press, 2008.
[15] F.W.J. Olver, Asymptotics and Special Functions, Academic Press, 1974.
[16] M.V. Fedoryuk, Asymptotic Analysis: Linear Ordinary Differential Equations, Springer, 1993.
[17] J. Wiersig, J. Main, Phys. Rev. E 77 (2008) 036205.